Molecular Basis of Enhanced Activity in Factor VIIa-Trypsin Variants Conveys Insights into Tissue Factor-mediated Allosteric Regulation of Factor VIIa Activity

Sorensen, Anders B.; Madsen, Jesper Jonasson; Svensson, L. Anders; Pedersen, Anette A.; Østergaard, Henrik; Overgaard, Michael T.; Olsen, Ole H.; Gandhi, Prafull S

Published in:
Journal of Biological Chemistry

Link to article, DOI:
10.1074/jbc.M115.698613

Publication date:
2016

Document Version
Peer reviewed version

JBC Papers in Press. Published on December 22, 2015 as Manuscript M115.698613
The latest version is at http://www.jbc.org/cgi/doi/10.1074/jbc.M115.698613

Molecular Basis of Enhanced Activity in Factor VIIa-Trypsin Variants Conveys Insights into Tissue Factor-Mediated Allosteric Regulation of Factor VIIa Activity

Anders B. Sorensen[1,2], Jesper J. Madsen*[1,3], L. Anders Svensson[1], Anette A. Pedersen[1], Henrik Østergaard[1], Michael T. Overgaard[2], Ole H. Olsen[1], Prafull S. Gandhi[1]

[1] Global Research, Novo Nordisk A/S, 2760 Måløv, Denmark
[2] Department of Chemistry and Bioscience, Aalborg University, 9220 Aalborg, Denmark
[3] Department of Chemistry, Technical University of Denmark, 2800 Kgs. Lyngby, Denmark
* Current affiliation: Department of Chemistry, The University of Chicago, Chicago, Illinois 60637, USA.

Running title: TF-mediated allostery in FVIIa

Correspondence: Prafull S. Gandhi, Protein Interaction, Novo Nordisk A/S, Novo Nordisk Park, G8.2.61, DK-2760 Måløv, Denmark. Tel.: +45 3079 9829. E-mail: pgan@novonordisk.com

Keywords: coagulation factor, allosteric regulation, x-ray crystallography, molecular dynamics, serine protease

Abstract

The complex of coagulation factor VIIa (FVIIa), a trypsin-like serine protease, and membrane bound tissue factor (TF) initiates blood coagulation upon vascular injury. Binding of TF to FVIIa promotes allosteric conformational changes in the FVIIa protease domain and improves its catalytic properties. Extensive studies have revealed two putative pathways for this allosteric communication. Here we provide further details of this allosteric communication by investigating FVIIa loop swap variants containing the 170-loop of trypsin that display TF-independent enhanced activity. Using x-ray crystallography, we show that the introduced 170-loop from trypsin directly interacts with the FVIIa active-site, stabilizing segment 215-217[a] and activation loop 3, leading to enhanced activity. Molecular dynamics simulations and novel fluorescence quenching studies support that segment 215-217 conformation is pivotal to the enhanced activity of the FVIIa variants. We speculate that the allosteric regulation of FVIIa activity by TF binding follows a similar path in conjunction with N-terminus insertion, suggesting a more complete molecular basis of TF-mediated allosteric enhancement of FVIIa activity.

Allosteric mechanisms play a vital role in the timely initiation and progression of the blood coagulation cascade. At the site of injury, membrane bound tissue factor (TF) interacts with zymogen coagulation factor VII (FVII) and its active form (FVIIa). The FVIIa:TF complex initiates the coagulation cascade by activating FIX and FX leading to thrombin generation and eventually wound healing (1). Conversion of FVII to FVIIa involves proteolytic cleavage at the R15-I16 peptide bond, producing a disulfide linked two chain molecule, with a light chain consisting of a phospholipid-interactive γ–carboxyglutamic acid (Gla) domain and two epidermal growth factor (EGF)-like domains, and a heavy chain tryspin-like protease domain (2) (Figure 1A). In trypsin, the N-terminus, formed upon activation, spontaneously enters the activation This key interaction leads to optimal alignment and architecture of the oxyanion hole and primary specificity pocket (S1) resulting in a mature active-site for substrate binding and catalysis (3). In FVIIa, the newly formed N-terminus fails to completely insert into the activation pocket (4), leading to a non-optimal configuration of the catalytic machinery, rendering FVIIa "zymogen-like" with inferior catalytic efficiency. TF binding allosterically corrects these defects in the catalytic

domain by stabilizing the 170-loop (amino acids 170-178) in conjunction with activation loops 1 through 3 (AL1-3), and promotes N-terminus insertion (Figure 1B) (5, 6). This transforms FVIIa into its catalytically competent form and increases amidolytic activity by 40-fold (7). Furthermore, TF ensures optimal orientation and positioning of the FVIIa catalytic domain above the membrane surface and generates exosites for incoming macromolecular substrates, thereby enhancing the proteolytic activity by ~ 10^5-fold (8, 9).

Previous studies have provided details of TF binding regions in the FVIIa light chain and on structural changes in the protease domain upon cofactor binding. However, the extent of TF-mediated structural changes is yet to be fully elucidated and key components of the allosteric pathways remain elusive (10). To further understand the molecular basis of TF-mediated allosteric regulation of FVIIa activity, we considered FVIIa variants displaying superior catalytic efficiency in the absence of TF - variants modified in the vicinity of either the 170-loop (11) or the activation pocket (7), or a variant with the 170-loop replaced by that of trypsin (FVIIa-Y_T) (12). Interestingly, FVIIa-Y_T displays a similar extent of N-terminus insertion as FVIIa-wild type (WT) in absence of TF; yet, FVIIa-Y_T displays improved catalytic efficiency. Recent studies with thrombin, another trypsin-like serine protease, reveal a highly plastic protease fold for the apo-form of thrombin that undergoes structural transitions upon cofactor binding (13–19). In particular, segment 215-217 was shown to be vital for substrate access and cofactor-mediated allosteric regulation, which may also be the case in TF-mediated allosteric regulation of FVIIa activity (20, 21).

We hypothesized that the improved catalytic efficiency of FVIIa-Y_T is due to stabilization of the 215-217 segment, with Y172 playing an important role. To test our hypothesis, we investigated the FVIIa-Y_T variant and two variants of FVIIa-Y_T, where this tyrosine is either replaced by serine (FVIIa-S_T) or phenylalanine (FVIIa-F_T) (Figure 1D). Data presented here confirm that Y172 stabilizes the 215-217 segment and AL3, in absence of TF, maturing the primary specificity pocket and enhancing catalytic efficiency independently of complete protease domain N-terminus insertion. Molecular dynamics (MD) simulations supported the experimental results and suggested the direct involvement of W215 in TF-mediated allosteric changes in the protease domain, further corroborated by fluorescence quenching studies and solvent accessible surface area (SASA) calculations. Based on these observations we hypothesize that stabilization of segment 215-217 in the open conformation is a key step in TF-mediated allosteric regulation of FVIIa.

Experimental Procedures

Materials – FFR (H-$_D$-Phe-Phe-Arg-chloro methylketone TFA-salt) was from Bachem (Basel, Switzerland). S-2288 ($_D$-Ile-Pro-Arg-pNA) was from Chromogenix (Mölndal, Sweden). All other chemicals were from Sigma Aldrich (GER) and of analytical grade or highest quality commercially available. Recombinant wild-type human FVIIa was prepared as described previously (11). Recombinant human soluble tissue factor 1-219 (sTF) was prepared as described (22), with the modification of using the reductase-deficient *E. coli* strain BL21 Origami (Novagen, GER). Factor Xa was purchased from Molecular Innovations (US).

Factor VII Mutagenesis and Protein Expression - Human wild-type FVII cDNA was cloned into a QMCF vector (Icosagen AS, Estonia) and all variants where generated using a PCR-based site-directed mutagenesis method with KOD Xtreme Hot Start DNA Polymerase (Novagen, US) or a QuikChange Lightning XL (Agilent, US) kit according to manufacturer's instructions. Introduction of the desired mutations was verified by DNA sequencing of the entire FVII cDNA region (MWG Biotech, GER). The QMCF Technology, a semi-stable episomal mammalian expression system, obtained from Icosagen AS (Estonia) was used for expression of the FVII variants in a QMCF CHO cell line (CHO-EBNALT85) and cells were cultivated according to manufacturer's instructions. During a

period of 3-4 weeks the transfected cell cultures were expanded to 2-10 L, and the media harvested by centrifugation and 0.22 μm filtration.

Protein Purification and Verification - For all FVII variants, expression medium was adjusted to pH 6.0, $CaCl_2$ added to 5 mM and benzamidine-HCl was added to a final concentration of 10 mM. All purification steps were performed using an Äkta Explorer system (GE Healthcare, US) and consisted of an immunoaffinity purification step (Gla-domain specific), performed as described (23), except at pH 6.0 using a histidine buffer and eluting with 20 mM EDTA. This was followed by a concentration and purification step using a prepacked 6 mL ResourceQ™ (GE Healthcare, US) column at pH 6.0, eluting with a step gradient to 100 mM NaCl, 60 mM $CaCl_2$ in 10 mM Histidine. Activation was performed by passing the protein solution through a custom-packed Tricon column (GE Healthcare, US) with Factor Xa coupled to Sepharose 4B FF CNBr (GE Healthcare, US). Protein identity was verified using intact ESI-TOF mass spectrometry and purity shown to be >95 % on a Novex 4-12 % SDS-PAGE (Life Technologies, US). The amount of active protein was determined by active-site titration using FFR, and measuring residual S-2288 activity (24).

Functional Evaluation of FVIIa 170-loop Variants - All functional assays were carried out in 50 mM Hepes, pH 7.4, 0.1 M NaCl, 5 mM $CaCl_2$, and 0.01 % Tween-20 (assay buffer) and monitored at 405 nm in a microplate reader (SpectraMax 340; Molecular Devices Corp., Sunnyvale, CA, U.S.A.) using a Nunc F96 well plate (Non-Treated-clear) with 200 uL assay volume at 25 °C. sTF binding studies using S-2288 were performed essentially as described (12), using 0-3 μM sTF. Kinetic parameters of S-2288 hydrolysis were determined for the FVIIa variants with 0-12.5 mM S-2288, and the K_i for inhibition by pABA was determined in a competitive activity assay using 1 mM S-2288 as described (11). Carbamylation of the N-terminus I16 was investigated by incubating in 0.2 M KNCO (Sigma Aldrich, US) and measuring residual activity at 1 mM S-2288 as described (11). All functional studies were performed in the absence or presence of 3 μM sTF. Data analysis and curve fitting was performed using GraphPad Prism 6.0.

FVIIa Variant Preparation, Crystallization and Data Collection - Preparation of samples for x-ray crystallography was performed by inhibiting FVIIa-Y_T, -S_T and -F_T with FFR and adding sTF in a 1:1 molar relationship. Protein integrity was verified using SDS-PAGE. Diffraction quality crystals were obtained using hanging-drop at 22°C with two different conditions, for FVIIa-Y_T and -F_T 0.1 M sodium citrate buffer at pH 5.1, 16.6 % PEG 3350 (Hampton Research, US), 12.5 % 1-Propanol, and for FVIIa-S_T 0.1 M cacodylate buffer at pH 5.6, and 12 % PEG 8000 (Hampton Research, US). All diffraction data was collected at MaxLab IV beam-line I911-3 (25). Data were integrated and scaled using the XDS package (26). Molecular replacement was performed with the Phenix.Phaser software (27) and a FVIIa-WT:sTF1-219-FFR complex as search model. The subsequent refinement and model building were performed using iterative cycles of Phenix.Refine (28) in the Phenix program package (29), utilizing MolProbity (30) and TLS (31), followed by computer graphic model corrections by the Coot software (32). The three generated structures were deposited in the Protein Databank (PDB) as FVIIa-Y_T (PDB # 4z6a), FVIIa-S_T (PDB # 4zmA), and FVIIa-F_T (PDB # 4ylq).

Acrylamide Tryptophan Quenching - Fluorescence intensity measurements were performed on a Cary Eclipse spectrofluorimeter (Agilent Technologies, US), equipped with a 4-cell magnetic stirrer sample holder and peltier element, using a set of 4 10x10 mm QS quartz cuvettes (Hellma Analytics, GER). 150 nM of FVIIa variant in assay buffer kept at 15, 25 or 37 °C was titrated with 0-0.5 M acrylamide using a volume-replacement approach by preparing two identical solutions for the titration, where one was spiked with 5.63 M acrylamide (Biorad, US). Data was collected with excitation at 295 nm (5 nm slit width) and emission at 330 nm (20 nm slit width), integration time was 0.5 sec. The collected data was baseline-corrected and inner filtering effects were addressed by a correction method for a right-

angled fluorescence setup (33), with the correction factor being $F_{corr}=F_{obs}\cdot 10^{0.125*[Acrylamide]}$, using a ε_{295} of 0.25 $M^{-1}cm^{-1}$ for acrylamide and a pathlength of fluorescence measurement of 0.5 cm. Stern-Volmer plots were generated and the data was analyzed using a dynamic collision quenching model (34) in GraphPad Prism 6.0:

$$\frac{F_0}{F} = 1 + K_{sv}[Q]$$

The observed correlation between the determined K_{sv} values and the calculated SASA values was evaluated using a Pearson correlation approach in GraphPad Prism 6.0 to determine whether it could be explained by random sampling (α=0.01).

Molecular Dynamics Simulations of FVIIa Variants - For MD simulations the FVIIa 170-loop variants were constructed using the x-ray crystallographic structure of FVIIa-Y_T as a template. For the S_T and F_T variants, Y172 was mutated to Ser and Phe, respectively, while preserving the sidechain rotamer of the template. FVIIa-WT was based on a representative structure of benzamidine-inhibited FVIIa (PDB # 1kli (35)). The complex of sTF 1-213 and FVIIa was constructed starting from PDB # 1dan as described (8), graciously provided by Ohkubo et al.. In all structures, the co-crystallized inhibitor was removed. 100 ns conventional MD simulations of the FVIIa-WT:sTF complex, FVIIa-WT, and the three FVIIa variants with the trypsin 170-loops were performed using the NAMD 2.7 software package (36) with the CHARMM27 force field (37) and the TIP3P water model (38). An integration time step of 1.0 fs was used for the velocity Verlet algorithm. Simulations were carried out at constant pressure (P = 1 atm), constant temperature (T = 310 K) controlled by the Langevin thermostat (damping coefficient: 5/ps) and the Nosé-Hoover Langevin piston barostat (39, 40), respectively. Throughout, anisotropic pressure coupling was applied for the barostat using piston damping coefficient of 5/ps, a piston period of 100 fs, and piston decay of 50 fs. Long-range electrostatic forces were calculated using the Particle Mesh Ewald method (41) using a grid spacing of approximately 1 Å and a fourth order spline for interpolation. Electrostatic forces were updated every fourth fs. Van der Waals interactions were cut off at 12 Å in combination with a switching function beginning at 10 Å. Periodic boundary conditions was applied in x-, y-, and z-directions. The potential energy in all systems was initially minimized using 500 steps of the conjugated gradient method.

*Solvent-Accessible Surface Area (SASA).*The SASA was calculated for all tryptophans in the simulated FVIIa variants during the entire time course at a probe radius of 1.4 Å using the standard implementation (*measure* command) in VMD (42). The same calculations were made for the crystal structures with FFR present. For graphical comparison of SASA values for W215 between variants, the data was smoothened using the Savistsky and Golay method in Graphpad Prism 6.0 with a window size of 10 and a 2nd degree polynomial.

Results

The 170-loop is Linked to Cofactor Binding and Amidolytic Activity - Previous studies have shown that conformation of the 170-loop is affected by the binding of TF to FVIIa (2, 6). In agreement, impairment of cofactor interaction was observed for the three FVIIa variants as assessed by the effect of soluble tissue factor (sTF) on FVIIa amidolytic activity (S-2288) (Figure 2A-D and Table 1). FVIIa-Y_T displayed an 84-fold compromise in its ability to bind to sTF, but could be fully stimulated by the addition of saturating sTF, reaching a higher final amidolytic activity than FVIIa-WT:sTF (Figure 2A, D). This indicates that the engineered 170-loop in FVIIa-Y_T selectively affects sTF binding, but is still able to mediate allosteric communication to the FVIIa active-site upon sTF binding. From the kinetics of S-2288 hydrolysis, we found that the increased FVIIa-Y_T activity at saturating sTF concentration was entirely due to an increased k_{cat} value, with no change in the K_M value compared with the FVIIa-WT:sTF complex (Figure 2D and Table 1). In addition, we reproduced the higher activity of FVIIa-Y_T without sTF, with an increase in k_{cat}/K_M of 8.3-fold over FVIIa-WT (12). The importance of Y172 was evident, as the removal of a single hydroxyl group (FVIIa-F_T) resulted in a markedly decreased potentiation of activity and a loss in sTF

affinity (Figure 2A-B and Table 1), with an accompanying reduction of the intrinsic activity to half that of FVIIa-WT (Figure 2C and Table 1). The FVIIa-S_T variant showed a partial rescue of sTF affinity (Table 1), maintaining a 4-fold higher intrinsic activity compared to FVIIa-WT, whereas the activity level at saturating sTF concentration, was significantly reduced (Figure 2A and Table 1). Independent surface plasmon resonance analysis confirmed sTF affinity values for the three FVIIa variants obtained by the amidolytic activity strategy (data not shown).

Inhibitor Binding Reveals Changes in S1 Pocket Maturation - To further investigate the effect of the engineered 170-loops on the active-site, we probed the S1 pocket by pABA binding, a small molecule inhibitor known to occupy the S1 pocket and oxyanion hole (35). Consistent with an immature S1 pocket, FVIIa-WT was poorly inhibited by pABA in the absence of sTF (K_i 1485 μM, Figure 3A and Table 1). The K_i values for FVIIa-Y_T and FVIIa-S_T were significantly decreased, in agreement with their increased amidolytic activity and a more mature S1 pocket (Table 1). FVIIa-F_T exhibited an intermediate K_i value. Binding of sTF to FVIIa-WT is known to mature the active-site (23), and resulted in a ~30-fold decreased K_i value (49.3 μM). At saturating sTF concentrations, FVIIa-WT, FVIIa-Y_T, FVIIa-S_T and FVIIa-F_T all reached similar K_i values (Figure 3A and Table 1), as anticipated for FVIIa-Y_T and FVIIa-S_T but not for FVIIa-F_T, due to its much lower activity towards S-2288. This suggests that FVIIa-F_T has a mature S1 pocket in the presence of sTF, but possibly impaired substrate binding in the S2-3 pockets.

Mutagenesis of the 170-loop Affects N-terminus Protection - A functional marker for FVIIa "zymogenicity" is the extent of N-terminus insertion, which can be perturbed by TF binding or by mutagenesis in FVIIa (7, 12). The carbamylation assay (Figure 3B and Table 1) correlates I16 (N-terminus) solvent exposure to residual activity, and has been successfully used to assess the extent of protease domain N-terminus insertion (4). In the absence of sTF, FVIIa-WT, FVIIa-Y_T and FVIIa-S_T showed similar levels of N-terminus protection, whereas the protection level was slightly decreased in FVIIa-F_T (Figure 3B). Addition of sTF had a pronounced effect on N-terminus insertion, with FVIIa-WT showing complete protection, whereas FVIIa-Y_T achieves very little protection, suggesting that the improved amidolytic activity observed for this variant is independent of complete N-terminus insertion. Interestingly, the FVIIa-S_T N-terminus is protected when compared to FVIIa-Y_T, correlating with the increased sTF affinity, whereas FVIIa-F_T showed the lowest level of protection gained from sTF addition, in agreement with a poor catalytic activity and sTF affinity.

Y172 Directly Stabilizes Segment 215-217 and AL3 - To investigate the conformation of the 170-loop from trypsin in FVIIa, we determined the x-ray crystal structure of the three variants with sTF and the irreversible active-site inhibitor H-$_D$-Phe-Phe-Arg-cmk (FFR) (2). The three FVIIa variants crystallized in identical space groups with highly similar unit cell dimensions allowing meaningful structural comparison. Data collection and refinement statistics are summarized in Table 2. Comparison of the protease domain of FVIIa-WT (PDB # 1dan (2)) and the three variants revealed the same structural topology (C_α $RMSD_{\text{protease domain, 241 residues}}$ of 0.27-0.39 Å) outside the immediate surroundings of the 170-loop and AL 2-3 (184-193 and 220–225) (Figure 4A-D). The FVIIa-Y_T map ($2F_0$-Fc) lacked electron density for the Ca^{2+} dependent Gla domain, presumably due to the presence of citrate in the crystallization condition and the cryo-protectant for this variant.
From the FVIIa-Y_T:sTF complex structure, it was evident that the trypsin 170-loop interacts with the active-site region. This was illustrated by hydrogen bonding from the hydroxyl group of Y172 to the backbone nitrogen of Q217 (3.1 Å) and the backbone carbonyl of F225 (2.5 Å), (Figure 4A and B). In addition, Y172 may further stabilize the 215-217 segment by favorable electrostatic aromatic interaction with W215 (closest ring carbons: 3.7-3.9 Å). In addition, the Y172 side chain displaces a water molecule (HOH_1) present in the FVIIa-WT structure, which may play a stabilizing role in the FVIIa-WT:sTF

complex (Figure 4B), supporting the increased amidolytic acitivty observed for the FVIIa-Y_T:sTF complex. It was also observed that a smaller serine at position 171, compared with glutamine in FVIIa-WT, seemed to enable the shorter 170-loop from trypsin to interact with the AL 3 backbone (Figure 5A).

The removal of the benzene, and shortening of the hydroxyl group placement in FVIIa-S_T resulted in a loss of electron density for residues S172 and P173 in the 170-loop (Figure 4C). This may result from competition of the shortened and possibly more mobile loop with a cacodylate ion found in both the FVIIa-S_T and FVIIa-WT structures (Figure 4C). The structural data obtained for FVIIa-F_T revealed 170-loop and AL 2-3 conformations very similar to that observed for FVIIa-Y_T, with F172 occupying the same position as Y172. The N-terminus, for the three variants, was inserted in the activation pocket as in the FVIIa-WT:sTF crystal structure, possibly due to the presence of sTF and FFR. In general, shortening of the 170-loop seemed to affect the structural integrity of the TF-binding helix (165-169) where the final turn of the helix was skewed for all three variants (Figure 5B), with FVIIa-Y_T and -F_T phi/psi angles of D167 and C168 outside the typical α-helix regions (Figure 5C). This correlated with the observed loss of sTF affinity and lower extent of N-terminus insertion for these variants, whereas FVIIa-S_T, with phi/psi angles closer to those of FVIIa-WT, exhibited improved sTF affinity and a higher extent of N-terminus insertion in the TF-bound complex. From these data it seems that the orientation of the 170-loop, and thus the structural integrity of TF-binding helix, alters the extent to which the N-terminus (I16) can be inserted into the activation pocket as a consequence of TF binding.

Molecular Dynamics Simulations Track W215 Movement – To allow for an unbiased observation of the dynamic behavior and a detailed understanding of the effects of Y172 on the protease domain, we performed 100 ns classical MD simulations for FVIIa-WT and the three variants, without active-site inhibitor and sTF. In addition, we also performed 100 ns classical MD simulations for FVIIa-WT in complex with sTF, without active-site inhibitor.

Our simulations show that AL1-3, including segment 215-217 which harbors W215 (Supplementary Videos S1-5), are highly flexible and undergo significant structural changes. The rearrangements are most pronounced in FVIIa-WT, where W215 not only releases from the aryl binding pocket (S3-S4), but the S1 pocket collapses entirely as indicated by the short distance between W215 and S195 (Figure 6A-C). This suggests that the FVIIa molecule undergoes a transition where the 215-217 segment moves from an open conformation, through an intermediate to a fully collapsed state, where especially W215 occludes the substrate-binding region (Figure 6A-C and D). In absence of sTF, this conformational transition from an open to a collapsed population is absent in FVIIa-Y_T, but is re-introduced in the FVIIa-S_T and -F_T variants (Figure 6D). Intriguingly, the 215-217 segment is stabilized in FVIIa-WT:sTF complex, in a similar manner to that observed for FVIIa-Y_T (Figure 6D). Additionally, it was observed that FVIIa-F_T displayed a significant collapse of the TF-binding helix in good agreement with the relatively low sTF affinity, and that W215 is released from the S3 pocket into a position where it can interfere with substrate binding to S2/S3 sites and conceivably cause the low amidolytic activity. Furthermore, it seems that this mechanism is independent of N-terminus insertion, as the salt bridge between the amino group of I16 and D194 was present for the duration of all simulations.

Fluorescence Quenching Shows Changes to Tryptophan Accessibility - To correlate the MD simulations with an experimentally measurable quantity, we calculated SASA values for all tryptophans in the FVIIa protease domain throughout the simulation time course (Figure 7A-C). The SASA values were compared with results from a fluorescence quenching assay reporting on tryptophan solvent exposure by monitoring the loss of overall tryptophan fluorescence intensity upon addition of acrylamide (Figure 7D) (34). According to the SASA calculations, three of the eight tryptophan residues (W61, W207 and W215) were partially or fully exposed (Figure 7B). This

agreed well with the fluorescence quenching data, where a significant level of quenching, or exposed tryptophans, was observed in FVIIa-WT (Figure 7D and Table 3). The observed linearity of the quenching data allowed for the assumption of a collision quenching mechanism to predict the Stern-Volmer quenching constant (K_{sv}) (43). In accordance with a collision quenching mechanism, increased quenching was observed with increasing temperatures (data not shown) (34).

Consistent with the distance plots (Figure 6D), W215 exhibited varying SASA values over the time course of the simulations for FVIIa-WT, -S_T and -F_T, whereas those of FVIIa-Y_T and FVIIa-WT:sTF showed lower and more stable levels (Figure 7C and Table 3). In agreement with these observations, FVIIa-Y_T showed a significant decrease in quenching at 15 °C, whereas FVIIa-F_T was only moderately protected and FVIIa-S_T showed a total quenching increase compared to FVIIa-WT (Figure 7D and Table 3). The SASA values for W215 correlated well (Pearson r value of 0.99 and $p<0.01$) with the K_{sv} values for the examined variants compared to W61/W207, where the relationship between the measured and experimental data was less pronounced (Figure 7E-G). A control experiment with FFR added to all variants gave the expected normalization of quenching values to that of inhibited FVIIa-WT. This was in good agreement with the calculated SASA values, reflecting complete shielding of W215, which should result in a significant decrease in overall quenching due to the large contribution from this residue to the total tryptophan surface accessible area (~33 %). These findings support that the acrylamide quenching is highly sensitive to the conformation of W215, even with the background signal from the remaining tryptophan residues.

Discussion

The TF-mediated allosteric regulation of FVIIa activity has been investigated for several decades generating a wealth of experimental evidence for two distinct allosteric pathways (Figure 1B). In the current model the two pathways have a suggested common origin at the FVIIa-TF interface, where especially the insertion of M164 from FVIIa into a pocket of TF has proven essential for the propagation of the allosteric signal to the FVIIa active-site (10, 23). From M164 the two pathways branch out, with pathway I moving through the TF-binding helix, to tether it and the 170-loop to the protease domain through R173 and G223 (24). Pathway II propagates through L163 and F225 to stabilize AL3 which in turn influences S185 in AL2, allowing N-terminus insertion which stabilizes a V17 to A221a interaction and the C191-C220 disulfide pair (44). Here we attempt to elaborate on these two pathways, and propose a more complete molecular basis of TF-mediated allosteric enhancement of FVIIa activity.

The crystal structure of FVIIa-Y_T in complex with sTF revealed that Y172, as in trypsin (45), is inserted into a cavity in the FVIIa protease domain forming key hydrogen bonds with Q217 and F225, and favorable electrostatic interaction with W215. These key interactions, missing in the FVIIa-S_T and -F_T crystal structures, result in stabilization of segment 215-217 and AL3 in FVIIa-Y_T. Both Q217 and F225 have been shown to be components of the two consensus TF-mediated allosteric pathways in FVIIa (5, 10, 46) which were recently suggested to encompass W215 (20). In addition, the hydroxyl group of Y172 displaces a water molecule (HOH_1, Figure 4A and B), found in the FVIIa-WT:sTF complex, which may result in a more stable hydrogen bond network leading to the observed higher activity for the FVIIa-Y_T:sTF complex. It is quite likely that the introduced 170-loop from trypsin stabilizes allosteric pathway 1 via Y172 interactions, in the absence of sTF, resulting in the increased amidolytic activity without complete N-terminus insertion. In presence of sTF, the inability of the FVIIa-Y_T protease domain N-terminus to completely insert in the activation pocket may stem from the strain imposed by Y172 on the 170-loop by making direct contacts with AL2 and 3. While these interactions stabilize the 215-217 segment and AL3 leading to improved activity, it may interfere with allosteric pathway II and have deleterious effect on the neighbouring AL1. AL1 and AL2, along with other key interactions, accommodate the N-terminus. Previous studies have shown the critical role of Y172 in engineering substrate specificity (47) and Na^+ mimicry (48) in trypsin, warranting future studies probing the influence of

Y172 on the conformation of segment 215-217 and the intrinsic activity of trypsin.

It has previously been reported that a five residue truncation of the FVIIa 170-loop, to the length found in trypsin, resulted in a 3-fold decrease in amidolytic activity (12). The FVIIa-S_T variant investigated here, has an identical 170-loop length, but showed a 4-fold increase in amidolytic activity. From the crystal structures of FVIIa-S_T and -Y_T (Figure 5A), it was evident that the additional changes relative to FVIIa-WT, specifically Q171 to serine, removed a clash with AL 2-3 allowing for the increased activity. This in turn suggests that shortening of the 170-loop in FVIIa-WT should result in gained activity if Q171 was concomitantly mutated to a non-clashing residue (e.g. Ser or Ala). A similar effect was not observed for FVIIa-F_T as the activity was decreased significantly compared to that of FVIIa-WT. It is possible that F172 may help stabilize the S1 pocket by locating itself into the cavity normally found in FVIIa, but is unable to stabilize the 215-217 segment, resulting in the observed decrease in amidolytic activity in combination with an increase in S1 pocket maturity. This effect became even more pronounced in the presence of sTF, with the cofactor still able to mature the S1 pocket to FVIIa-WT levels, through the proposed pathway II (10), but unable to potentiate amidolytic activity. The unfavorable conformation of the TF-binding helix may explain this, as it is likely to result in the low extent of N-terminus insertion which, without the effects of Y172, results in a significant destabilization of the whole activation pocket and the active-site (5). In conclusion, despite incomplete N-terminus insertion, a combination of several factors appear to contribute to the activity gain of FVIIa-Y_T, including 170-loop shortening, removal of a Q171 clash, direct stabilization of 215-217 segment and AL3 through Y172, and the displacement of a water molecule which may enhance an allosteric pathway from L163 to the 215-217 segment.

The MD simulations allowed tracking of segment 215-217 movement in the three FVIIa-170-loop variants and FVIIa-WT. A clear picture emerged of FVIIa-Y_T being able to retain the "open" active conformation, whereas FVIIa-S_T, FVIIa-F_T and FVIIa-WT collapsed into inactive "closed" states, with W215 occluding the active-site. Addition of sTF to FVIIa-WT stabilized segment 215-217 in the active "open" conformation, very similar to that of FVIIa-Y_T. This is in agreement with recent hydrogen-deuterium exchange mass spectrometry (20), where an increase in W215 backbone amide protection was seen upon sTF addition. The combined approach of SASA calculation and in solution quenching used here allowed an elaboration on these observations. The approach showed a lower degree of quenching for the more active variants, correlating with the SASA calculations, supporting the suggested activity-regulating mechanism observed in the MD simulations for the 170-loop swap variants. From these observations, we speculate that the final mechanism, in the conversion of FVIIa into its catalytically competent state, involves segment 215-217 moving from a collapsed to a more open conformation upon TF binding, allowing substrate access to the active-site. The two allosteric pathways in FVIIa (10) may work in unison to allow for the stabilization of segment 215-217 in an open conformation, since both stabilization of the 170-loop and AL1-3, through insertion of the N-terminus, are needed to maintain FVIIa in a fully catalytically competent state. The exact distribution of the suggested open and collapsed states in FVIIa, their relation to the N-terminus insertion event and whether this distribution is affected by binding of TF remains to be explored.

The ability of the trypsin 170-loop to stabilize the 215-217 segment in FVIIa prompted an investigation of the conformation surrounding the 170-loop and the active-site in other trypsin-like proteases (Figure 8). An interesting pattern emerges from the analyzed crystal structures, with FVIIa and trypsin located at opposite ends of the spectra with regards to reported activity. Three of the proteases involved in blood coagulation, factor IXa (49), factor Xa (50) and thrombin (51), all show possible stabilization of segment 215-217 via a conserved water hydrogen bond network between the E217 carboxyl group and the 170-loop. This mode of stabilization may however be more transient than the Y172-mediated mechanism observed in trypsin. Ethylene glycol improves Factor IXa activity ~20-fold (52) and

may mimic the role of Y172. In Factor Xa, the presence of three consecutive serines (171-173) may mitigate the mobility of the water network (48) leading to higher intrinsic activity of this protease (53). In thrombin, recent work has shown that the apo-form of thrombin is highly flexible (17) and exists in an open/collapsed equilibrium controlled by the position of the 215-217 segment (16, 18, 54), where the addition of Na^+ shifts the equilibrium in favor of the open form. We speculate that in the apo-form, the water network in thrombin facilitates a 170-loop mediated stabilization of segment 215-217. In chymotrypsin, W172 makes a weak electrostatic interaction with the backbone of P225 and may stabilize the 215-217 segment by an edge-face stacking interaction with W215 (55). From the structures reviewed here we speculate that stabilization of the 215-217 segment in an open conformation, through 170-loop interactions, could be a recurring theme in trypsin-like proteases (56), and that the structural mechanism behind this has diverged through evolution. This may accommodate the development of allosteric regulatory control, as decreased intrinsic activity creates the need for co-factors to achieve full activity. Such intricate mechanisms, in conjunction with the generation of new exosites due to co-factor binding, allow for the necessary control of protease activity in the complex enzymatic cascades of blood coagulation.

Acknowledgements: The authors thank Michael P. Petersen and Anette S. Petersen for excellent technical assistance. We also thank Hanne Grøn, Grant E. Blouse and Egon Persson for valuable scientific discussions and comments. ABS and JJM were supported by grants from the Danish Agency for Science, Technology and Innovation and the Novo Nordisk R&D Science Talent Attraction and Recruitment (STAR) program. The three crystal structures presented here were deposited at the Protein Databank with accession codes 4z6a, 4zma and 4ylq

Conflict of interest: ABS, LAS, AAP, HØ, OHO and PSG are employees of Novo Nordisk A/S.

Author Contributions: ABS designed the research, conducted experiments, analyzed the results, and wrote and revised the manuscript. JJM designed the research, conducted the molecular dynamics simulations, and wrote the manuscript. LAS and AAP supported the experiments and analyzed results. HØ, MTO, and OHO designed the research, reviewed the results, and revised the manuscript. PSG designed the research, reviewed the results, and wrote and revised the manuscript.

References

1. Davie, E. W., Fujikawa, K., and Kisiel, W. (1991) The coagulation cascade: initiation, maintenance, and regulation. *Biochemistry*. **30**, 10363–70
2. Banner, D., D'Arcy, A., Chene, C., Winkler, F., Guha, A., Konigsberg, W. H., Nemerson, Y., and Kirchhofer, D. (1996) The crystal structure of the complex of blood coagulation factor VIIa with soluble tissue factor. *Nature*. **380**, 41–6
3. Huber, R., and Bode, W. (1978) Structural basis of the activation and action of trypsin. *Acc. Chem. Res.* **266**, 114–122
4. Higashi, S., Nishimura, H., Aita, K., and Iwanaga, S. (1994) Identification of regions of bovine factor VII essential for binding to tissue factor. *J. Biol. Chem.* **269**, 18891–8
5. Rand, K. D., Andersen, M. D., Olsen, O. H., Jørgensen, T. J. D., Ostergaard, H., Jensen, O. N., Stennicke, H. R., and Persson, E. (2008) The origins of enhanced activity in factor VIIa analogs and the interplay between key allosteric sites revealed by hydrogen exchange mass spectrometry. *J. Biol. Chem.* **283**, 13378–87
6. Pike, A. C., Brzozowski, A. M., Roberts, S. M., Olsen, O. H., and Persson, E. (1999) Structure of human factor VIIa and its implications for the triggering of blood coagulation. *Proc. Natl. Acad. Sci. U. S. A.* **96**, 8925–30
7. Persson, E., Kjalke, M., and Olsen, O. H. (2001) Rational design of coagulation factor VIIa variants with substantially increased intrinsic activity. *Proc. Natl. Acad. Sci. U. S. A.* **98**, 13583–8
8. Ohkubo, Y. Z., Morrissey, J. H., and Tajkhorshid, E. (2010) Dynamical view of membrane binding and complex formation of human factor VIIa and tissue factor. *J. Thromb. Haemost.* **8**, 1044–53
9. McCallum, C. D., Hapak, R. C., Neuenschwander, P. F., Morrissey, J. H., and Johnson, A. E. (1996) The location of the active site of blood coagulation factor VIIa above the membrane surface and its reorientation upon association with tissue Factor: A fluorescence energy transfer study. *J. Biol. Chem.* **271**, 28168–28175
10. Persson, E., and Olsen, O. H. (2011) Allosteric activation of coagulation factor VIIa. *Front. Biosci.* **16**, 3156–3163
11. Persson, E., Bak, H., Østergaard, A., and Olsen, O. H. (2004) Augmented intrinsic activity of Factor VIIa by replacement of residues 305, 314, 337 and 374: evidence of two unique mutational mechanisms of activity enhancement. *Biochem. J.* **379**, 497–503
12. Soejima, K., Mizuguchi, J., Yuguchi, M., Nakagaki, T., Higashi, S., and Iwanaga, S. (2001) Factor

VIIa modified in the 170 loop shows enhanced catalytic activity but does not change the zymogen-like property. *J. Biol. Chem.* **276**, 17229–35

13. Gandhi, P. S., Chen, Z., Mathews, F. S., and Di Cera, E. (2008) Structural identification of the pathway of long-range communication in an allosteric enzyme. *Proc. Natl. Acad. Sci. U. S. A.* **105**, 1832–7
14. Pozzi, N., Vogt, A. D., Gohara, D. W., and Di Cera, E. (2012) Conformational selection in trypsin-like proteases. *Curr. Opin. Struct. Biol.* **22**, 421–31
15. Bah, A., Garvey, L. C., Ge, J., and Di Cera, E. (2006) Rapid kinetics of Na+ binding to thrombin. *J. Biol. Chem.* **281**, 40049–56
16. Niu, W., Chen, Z., Gandhi, P. S., Vogt, A. D., Pozzi, N., Pelc, L. a., Zapata, F., and Di Cera, E. (2011) Crystallographic and kinetic evidence of allostery in a trypsin-like protease. *Biochemistry*. **50**, 6301–6307
17. Lechtenberg, B. C., Johnson, D. J. D., Freund, S. M. V, and Huntington, J. A. (2010) NMR resonance assignments of thrombin reveal the conformational and dynamic effects of ligation. *Proc. Natl. Acad. Sci. U. S. A.* **107**, 14087–92
18. Vogt, A. D., Chakraborty, P., and Di Cera, E. (2015) Kinetic Dissection of the Pre-existing Conformational Equilibrium in the Trypsin Fold. *J. Biol. Chem.* **290**, 22435–22445
19. Huntington, J. A., and Esmon, C. T. (2003) The molecular basis of thrombin allostery revealed by a 1.8 Å structure of the "slow" form. *Structure*. **11**, 469–479
20. Song, H., Olsen, O. H., Persson, E., and Rand, K. D. (2014) Sites involved in intra- and interdomain allostery associated with the activation of factor VIIa pinpointed by hydrogen-deuterium exchange and electron transfer dissociation mass spectrometry. *J. Biol. Chem.* **289**, 35388–35396
21. Madsen, J. J., Persson, E., and Olsen, O. H. (2015) Tissue factor activates allosteric networks in factor VIIa through structural and dynamic changes. *J. Thromb. Haemost.* **13**, 262–267
22. Freskgård, P. O., Olsen, O. H., and Persson, E. (1996) Structural changes in factor VIIa induced by Ca2+ and tissue factor studied using circular dichroism spectroscopy. *Protein Sci.* **5**, 1531–40
23. Persson, E., Nielsen, L. S., and Olsen, O. H. (2001) Substitution of aspartic acid for methionine-306 in Factor VIIa abolishes the allosteric linkage between the active site and the binding interface with tissue factor. *Biochemistry*. **40**, 3251–3256
24. Persson, E., and Olsen, O. H. (2009) Activation loop 3 and the 170 loop interact in the active conformation of coagulation factor VIIa. *FEBS J.* **276**, 3099–109
25. Ursby, T., Unge, J., Appio, R., Logan, D. T., Fredslund, F., Svensson, C., Larsson, K., Labrador,

A., and Thunnissen, M. M. G. M. (2013) The macromolecular crystallography beamline I911-3 at the MAX IV laboratory. *J. Synchrotron Radiat.* **20**, 648–653

26. Kabsch, W. (2010) Xds. *Acta Crystallogr. D. Biol. Crystallogr.* **66**, 125–32
27. McCoy, A. J., Grosse-Kunstleve, R. W., Adams, P. D., Winn, M. D., Storoni, L. C., and Read, R. J. (2007) Phaser crystallographic software. *J. Appl. Crystallogr.* **40**, 658–674
28. Afonine, P. V., Grosse-Kunstleve, R. W., Echols, N., Headd, J. J., Moriarty, N. W., Mustyakimov, M., Terwilliger, T. C., Urzhumtsev, A., Zwart, P. H., and Adams, P. D. (2012) Towards automated crystallographic structure refinement with phenix.refine. *Acta Crystallogr. Sect. D Biol. Crystallogr.* **68**, 352–367
29. Adams, P. D., Afonine, P. V, Bunkóczi, G., Chen, V. B., Davis, I. W., Echols, N., Headd, J. J., Hung, L.-W., Kapral, G. J., Grosse-Kunstleve, R. W., McCoy, A. J., Moriarty, N. W., Oeffner, R., Read, R. J., Richardson, D. C., Richardson, J. S., Terwilliger, T. C., and Zwart, P. H. (2010) PHENIX: a comprehensive Python-based system for macromolecular structure solution. *Acta Crystallogr. D. Biol. Crystallogr.* **66**, 213–21
30. Davis, I. W., Leaver-Fay, A., Chen, V. B., Block, J. N., Kapral, G. J., Wang, X., Murray, L. W., Arendall, W. B., Snoeyink, J., Richardson, J. S., and Richardson, D. C. (2007) MolProbity: All-atom contacts and structure validation for proteins and nucleic acids. *Nucleic Acids Res.* **35**, 375–383
31. Winn, M. D., Murshudov, G. N., and Papiz, M. Z. (2003) Macromolecular TLS refinement in REFMAC at moderate resolutions. *Methods Enzymol.* **374**, 300–321
32. Emsley, P., Lohkamp, B., Scott, W. G., and Cowtan, K. (2010) Features and development of Coot. *Acta Crystallogr. Sect. D Biol. Crystallogr.* **66**, 486–501
33. Lutz, H., and Luisi, P. L. (1983) Correction for inner filter effects in fluorescence spectroscopy. *Helv. Chim. Acta*. **66**, 1929–1935
34. Lakowicz, J. (2007) *Principles of fluorescence spectroscopy*, 3rd Ed., Springer, NY
35. Sichler, K., Banner, D. W., D'Arcy, A., Hopfner, K. P., Huber, R., Bode, W., Kresse, G.-B., Kopetzki, E., and Brandstetter, H. (2002) Crystal structures of uninhibited Factor VIIa link its cofactor and substrate-assisted activation to specific interactions. *J. Mol. Biol.* **322**, 591–603
36. Phillips, J. C., Braun, R., Wang, W., Gumbart, J., Tajkhorshid, E., Villa, E., Chipot, C., Skeel, R. D., Kalé, L., and Schulten, K. (2005) Scalable molecular dynamics with NAMD. *J. Comput. Chem.* **26**, 1781–802
37. Mackerell, A. D., Bashford, D., Bellott, M., Dunbrack, R. L., Evanseck, J. D., Field, M. J., Fischer, S., Gao, J., Guo, H., Ha, S., Kuchnir, L., Kuczera, K., Lau, F. T. K., Mattos, C., Michnick,

S., Ngo, T., Nguyen, D. T., Prodhom, B., Reiher, W. E., Roux, B., Schlenkrich, M., Smith, J. C., Stote, R., Straub, J., Watanabe, M., Wio, J., Yin, D., and Karplus, M. (1998) All-Atom empirical potential for molecular modeling and dynamics studies of proteins. *J. Phys. Chem. B*. **5647**, 3586–3616

38. Jorgensen, W. L., Chandrasekhar, J., Madura, J. D., Impey, R. W., and Klein, M. L. (1983) Comparison of simple potential functions for simulating liquid water. *J. Chem. Phys.* **79**, 926
39. Martyna, G. J., Tobias, D. J., and Klein, M. L. (1994) Constant pressure molecular dynamics algorithms. *J. Chem. Phys.* **101**, 4177
40. Feller, S. E., Zhang, Y., Pastor, R. W., and Brooks, B. R. (1995) Constant pressure molecular dynamics simulation: The Langevin piston method. *J. Chem. Phys.* **103**, 4613
41. Essmann, U., Perera, L., Berkowitz, M. L., Darden, T., Lee, H., and Pedersen, L. G. (1995) A smooth particle mesh Ewald method. *J. Chem. Phys.* **103**, 8577–8593
42. Humphrey, W., Dalke, A., and Schulten, K. (1996) VMD: visual molecular dynamics. *J. Mol. Graph.* **14**, 33–38
43. Eftink, R., and Ghiron, C. A. (1981) Fluorescence quenching studies with proteins. *Anal. Biochem.* **227**, 199–227
44. Olsen, O. H., Rand, K. D., Østergaard, H., and Persson, E. (2007) A combined structural dynamics approach identifies a putative switch in factor VIIa employed by tissue factor to initiate blood coagulation. *Protein Sci.* **16**, 671–82
45. Gaboriaud, C., Serre, L., Guy-Crotte, O., Forest, E., and Fontecilla-Camps, J. C. (1996) Crystal structure of human trypsin 1: unexpected phosphorylation of Tyr151. *J. Mol. Biol.* **259**, 995–1010
46. Petrovan, R. J., and Ruf, W. (2000) Role of residue Phe225 in the cofactor-mediated, allosteric regulation of the serine protease coagulation factor VIIa. *Biochemistry*. **39**, 14457–63
47. Hedstrom, L., Perona, J. J., and Rutter, W. J. (1994) Converting trypsin to chymotrypsin: Residue 172 is a substrate specificity determinant. *Biochemistry*. **33**, 8757–8763
48. Page, M. J., Bleackley, M. R., Wong, S., MacGillivray, R. T. a, and DiCera, E. (2006) Conversion of trypsin into a Na+-activated enzyme. *Biochemistry*. **45**, 2987–2993
49. Zögg, T., and Brandstetter, H. (2009) Structural basis of the cofactor- and substrate-assisted activation of human coagulation factor IXa. *Structure*. **17**, 1669–1678
50. Salonen, L. M., Bucher, C., Banner, D. W., Haap, W., Mary, J. L., Benz, J., Kuster, O., Seiler, P., Schweizer, W. B., and Diederich, F. (2009) Cation-π interactions at the active site of factor Xa: Dramatic enhancement upon stepwise N-alkylation of ammonium ions. *Angew. Chemie - Int. Ed.* **48**, 811–814

51. Pineda, A. O., Carrell, C. J., Bush, L. A., Prasad, S., Caccia, S., Chen, Z.-W., Mathews, F. S., and Di Cera, E. (2004) Molecular dissection of Na+ binding to thrombin. *J. Biol. Chem.* **279**, 31842–53

52. Stürzebecher, J., Kopetzki, E., Bode, W., and Hopfner, K. P. (1997) Dramatic enhancement of the catalytic activity of coagulation factor IXa by alcohols. *FEBS Lett.* **412**, 295–300

53. Hopfner, K. P., Brandstetter, H., Karcher, A., Kopetzki, E., Huber, R., Engh, R. A., and Bode, W. (1997) Converting blood coagulation factor IXa into factor Xa: dramatic increase in amidolytic activity identifies important active site determinants. *EMBO J.* **16**, 6626–6635

54. Carter, W. J., Myles, T., Gibbs, C. S., Leung, L. L., and Huntington, J. a. (2004) Crystal Structure of Anticoagulant Thrombin Variant E217K Provides Insights into Thrombin Allostery. *J. Biol. Chem.* **279**, 26387–26394

55. Cohen, G. H., Silverton, E. W., and Davies, D. R. (1981) Refined crystal structure of gamma-chymotrypsin at 1.9 A resolution. Comparison with other pancreatic serine proteases. *J. Mol. Biol.* **148**, 449–479

56. Gohara, D. W., and Di Cera, E. (2011) Allostery in trypsin-like proteases suggests new therapeutic strategies. *Trends Biotechnol.* **29**, 577–85

Footnotes
The abbreviations used are: TF, Tissue Factor; sTF, soluble tissue factor 1-219; FVIIa, activated coagulation factor VIIa; FVII, zymogen coagulation factor VII; Gla-domain, γ–carboxyglutamic acid domain; EGF, epidermal growth factor; AL1-3, activation loops 1 through 3; MD, molecular dynamics; SASA, solvent accessible surface area; FFR, H-$_D$-Phe-Phe-Arg-chloromethylketone; S-2288, $_D$-Ile-Pro-Arg-pNA; PDB, Protein Databank; V_{int}, initial velocity;

Figure legends

Figure 1 Overview of the FVIIa-WT:sTF Complex and Variant nomenclature
(A) Full view of the FVIIa-WT:sTF (PDB # 1dan) complex with the FVIIa protease domain in grey, light chain in blue, sTF in orange, Ca^{2+} ions in yellow, and the active-site triad in magenta. Phospholipid-interactive γ–carboxyglutamic acid (Gla) domain and epidermal growth factor (EGF)-like domain.
(B) FVIIa-WT protease domain with the 170-loop (170-178), activation loop (AL) 1 (142-152), 2 (184-193) and 3 (220-225) in sand. Residues suggested to be involved in TF-induced enhancement in FVIIa activity through allosteric pathway I (blue) and II (green) shown with connecting dotted lines. Common residues for both pathways, from Y94 in TF are shown in red. FFR is shown in black. New sections of the pathways suggested here are marked with red fully-drawn lines.
(C) FFR inhibitor (black) shown in the active-site of FVIIa with substrate subsites 1 and 2 marked
(D) Sequence alignment of FVIIa-WT, Trypsin and the FVIIa variants with mutations highlighted (orange).

Figure 2 Cofactor Binding and Amidolytic Activity of FVIIa Variants
(A) Initial velocity (V_{int}) of 1 mM S-2288 hydrolysis by 15 nM FVIIa-WT (O) in black, FVIIa-Y_T (◊) in orange, FVIIa-S_T (□) in cyan, FVIIa-F_T (Δ) in green as a function of sTF concentration (0-3 μM), data shown as mean high/low error bars, n=2, and fitted with a quadratic equilibrium equation.
(B) sTF fractional saturation of FVIIa variants using S-2288 activity. Data normalized and fitted with a quadratic equilibrium equation. Mean +/- high/low error bars, n=2.
(C-D) Initial velocity values for hydrolysis of S-2288, without or with 3 μM sTF. Data fitted with a Michaelis-Menten equation using non-linear regression. Mean high/low error bars, n=2, at 25°C.

Figure 3 Functional Characterization of FVIIa Variants.
(A) Titration of 10-100 nM FVIIa-WT (O) in black, FVIIa-Y_T (◊) in orange, FVIIa-S_T (□) in cyan, FVIIa-F_T (Δ) in green with 0-30 mM pABA inhibitor, normalized to residual activity in the presence of 1 mM S-2288. Data were fitted with a competitive inhibition equation. Mean high/low error bars n=2. Without sTF (top panel), with 3 μM sTF (bottom panel).
(B) Carbamylation assay with 0.2 M KNCO monitoring residual S-2288 activity as a function of time, fitted with a single exponential decay function. Mean high/low error bars, n=2, at 25°C.

Figure 4 Structural Analysis Reveals an Important Role of Y172
(A) Comparison of FVIIa-WT (PDB # 1dan, dark blue) and FVIIa-Y_T (orange) showing the insertion of Y172 which displaces HOH_1. Water molecules found in the region of activation loops 2 and 3 (AL2-3) in FVIIa-WT are shown as blue spheres with all density contoured at 1.0 σ level.
Crystal structures of (B) FVIIa-Y_T (orange), (C) FVIIa-S_T (cyan) and (D) FVIIa-F_T (green) in complex with sTF and an active-site inhibitor (FFR). Water molecules in the variants around the AL2-3 region are shown as spheres in their respective colors and for FVIIa-WT in blue. Hydrogen bonding from the OH group of Y172 to Q217/F225 is shown with red dashed lines, together with possible stacking interaction with W215. The N-terminus was found to be in place in all variants, illustrated by the red-dotted line from

D194 to I16. The cacodylate ion present in the FVIIa-WT structure is found in FVIIa-S_T but not in FVIIa-Y_T and -F_T as the pocket is occupied by Tyr/Phe.

Figure 5 Structural effects of 170-loop substitution
(A) Alignment of the 170-loop from FVIIa-WT and FVIIa-Y_T showing removal of the possible Q171 clash in FVIIa-Y_T by replacement to a serine at position 171.
(B) Alignment of the 170-loop main chain of FVIIa-WT, -Y_T, -S_T and -F_T, showing changes to the main chain hydrogen bonding network of the TF-binding α-helices in the variants. Red dashed lines depict the backbone hydrogen bonding network of the FVIIa-WT α-helix.
(C) Calculated phi/psi angles for amino acids T165-C168 in the beginning of the TF-binding helix, with grey shaded areas being ideal phi/psi angles as published by EMBL and * marks angles outside the ideal region.

Figure 6 W215 Location in Relation to the Active-site
Representative conformations of segment 215-217 measured as W215 relative distances to the catalytic triad; (A) open, (B) intermediate and (C) collapsed, each state is depicted on the scatter plots with their respective letter.
(D) Scatter plots of W215 distance to the active residues H57 and S195. Data from 0-33 ns is in light red, 33-67 ns in light blue and 67-100 ns in black. Single data points from 1 ns shown as a blue filled dot, 50 ns in green, and 100 ns in red. The calculated trajectories are available as supplementary data (Supplementary Movie S1-S5)

Figure 7 Evaluation of Tryptophan Surface Accessibility
(A) Conformations of W215 in FVIIa-WT during MD simulations with Van der Waals surface area in red in an open (0 ns), intermediate (73 ns) and collapsed conformation with collapsed S1 pocket (99 ns)
(B) Plot of the calculated SASA values for all tryptophans of the protease domain during the simulation of FVIIa-WT. W29 (black), W51 (orange), W61 (green), W141 (blue), W207 (purple), W215 (red) and W237 (grey)
(C) Calculated SASA values of W215 for all FVIIa variants during 100 ns MD simulations, smoothened using a Savistsky and Golay algorithm. FVIIa-WT (black), FVIIa-WT:sTF (blue), FVIIa-Y_T (orange), FVIIa-S_T (cyan), FVIIa-F_T (green).
(D) Stern-Volmer plot for the FVIIa variants as a function of acrylamide concentration. FVIIa-WT (O, black), FVIIa-Y_T (◊, orange), FVIIa-S_T (□, cyan) and FVIIa-F_T (Δ, green) in the presence (dotted-line) or absence (full-line) of FFR. Mean +/- SD error bars, n=2-4 at 15°C.
(E-G) Scatter plot and correlation between the estimated K_{sv} constants and trajectory-averaged SASA values for W61, W207 and W215 for each individual FVIIa variant. SASA values with FFR present were calculated from the obtained crystal structures. The error bars indicating the standard deviation are shown for both abscissa and ordinate. A linear regression has been overlaid for W215 to illustrate correlation, which was statistically evaluated using a Pearson test.

Figure 8 Overview of 170-loop mediated Active-site Stabilization in Trypsin-like Serine Proteases
(A) Alignment of the selected proteases with residues corresponding to Y172, W215, D217 and P225 in trypsin shown in red. Structural overview of plausible 170-loop stabilization of the 215-217 segment in factor VIIa:sTF (B, PDB # 1dan) with cacodylate (CAC), factor IXa (C, PDB # 2wph in dark and PDB # 2wpk light orange with ethylene glycol (EG) in grey), factor Xa (D, PDB # 2jkh) with Na^+ in grey, thrombin (E, PDB # 1sgi in light and PDB # 1sg8 in dark red) with Na^+ in grey and coordinated waters in red, trypsin (F, PDB # 1trn), mouse chymotrypsin (G, PDB # 2gch). Water molecules for all structures are shown as blue spheres with electron density contoured at σ=0.7, with water hydrogen bonds (2.5-3.5Å) as red-dotted lines and grey for ethylene glycol.

Tables

	S-2288 K_M [mM]	S-2288 k_{cat} [s^{-1}]	k_{cat}/K_M [s^{-1}/mM]	pABA K_i [μM]	KNCO $t_{½}$ [min]
			-sTF		
FVIIa-WT	8.9 (0.4)	7.7 (0.2)	0.9 (0.02)	1485.0 (87.7)	43.9 (1.0)
FVIIa-Y_T	4.0 (0.1)	30.4 (0.5)	7.5 (0.2)	97.6 (10.1)	40.8 (0.5)
FVIIa-S_T	5.3 (0.2)	19.3 (0.3)	3.6 (0.1)	190.4 (13.1)	43.8 (0.6)
FVIIa-F_T	15.4 (1.3)	6.8 (0.4)	0.4 (0.01)	490.3 (46.3)	32.4 (0.7)
			+sTF		
FVIIa-WT	1.2 (0.03)	34.6 (0.2)	28.0 (0.4)	49.3 (1.8)	536.2 (39.6)
FVIIa-Y_T	1.2 (0.02)	41.7 (0.2)	34.4 (0.5)	24.7 (1.2)	56.7 (0.9)
FVIIa-S_T	3.0 (0.06)	37.1 (0.3)	12.4 (0.2)	41.7 (1.3)	159.0 (4.8)
FVIIa-F_T	5.6 (0.1)	21.6 (0.3)	3.9 (0.1)	69.5 (3.7)	37.1 (0.7)

Table 1 Functional Investigation of 170-loop Variants
Dissociation constants ($K_{d,app}$) for FVIIa-WT (1.2 ± 0.3), -Y_T (101.6 ±4.1), -S_T (34.2 ± 2.0) and -F_T (231.1 ± 22.8) determined by S-2288 activity measurements. S-2288 amidolytic kinetic constants, pABA inhibition values and carbamylation half-life as means with calculated SEM (n=2), at 25°C.

	FVIIa-Y_T	FVIIa-S_T	FVIIa-F_T
PDB ID	4z6a	4zma	4ylq
Data collection			
Wavelength (Å)	1.00	1.00	1.00
Space group	$P2_12_12_1$	$P2_12_12_1$	$P2_12_12_1$
Cell dimensions			
a, *b*, *c* (Å)	67.0 81.7 124.6	66.2 80.9 125.8	71.3 80.0 123.4
α, β, γ (°)	90 90 90	90 90 90	90 90 90
Molecules/Asymetric unit	1	1	1
Resolution Range (Å)	29.1-2.25 (2.33-2.25)[a]	29.8-2.3 (2.4-2.3)	33.6-1.4 (1.45-1.40)
Total reflections	155,080	104,023	1,008,907
Unique reflections	32,039	29,510	138,937
Completeness (%)	97.0 (81.0)	96.1 (87.4)	1.00 (0.98)
R_{merge}	0.14 (1.4)	0.16 (1.9)	0.09 (2.1)
$I/\sigma I$	10.0 (0.97)	8.7 (0.78)	14.1 (0.83)
Refinement			
Resolution (Å)	29.1-2.25	29.8-2.3	33.6-1.4
R_{work}/R_{free}	0.19/0.24	0.24/0.29	0.14/0.17
Reflections[b] (working/test)	32039/1605	29510/1500	138932/6917
R.m.s. deviations			
Bond lengths (Å)	0.003	0.002	0.024
Bond angles (°)	0.83	0.59	4.09
Wilson B-factor	36.9	33.4	15.3
Average atomic B-factors			
Protein	45.6	38.2	22.4
Ligands	59.9	54.8	46.0
Solvent	38.7	33.8	33.2
Ramachandran			
favored (%)	97.2	94.6	97.5
allowed (%)	2.8	5.4	2.5
outliers (%)	0	0	0

Table 2 Data collection and Refinement Statistics of X-ray Crystallography.
[a]Highest resolution shell
[b]Cut-off used in refinement was F > 0σF

	K_{sv} [M^{-1}] -FFR	K_{sv} [M^{-1}] +FFR	W215 SASA [$Å^2$]
FVIIa-WT	2.5 (0.008)	1.9 (0.01)	112 (33)
FVIIa-Y_T	2.3 (0.006)	1.8 (0.006)	77 (14)
FVIIa-S_T	2.6 (0.006)	1.9 (0.009)	110 (33)
FVIIa-F_T	2.4 (0.004)	1.8 (0.01)	85 (29)

Table 3 Tryptophan Surface Accessibility
Calculated mean solvent accessible surface area (SASA) from MD simulations and acrylamide Stern-Volmer constants (K_{sv}) as means with calculated SEM (n=2-4).

Figures

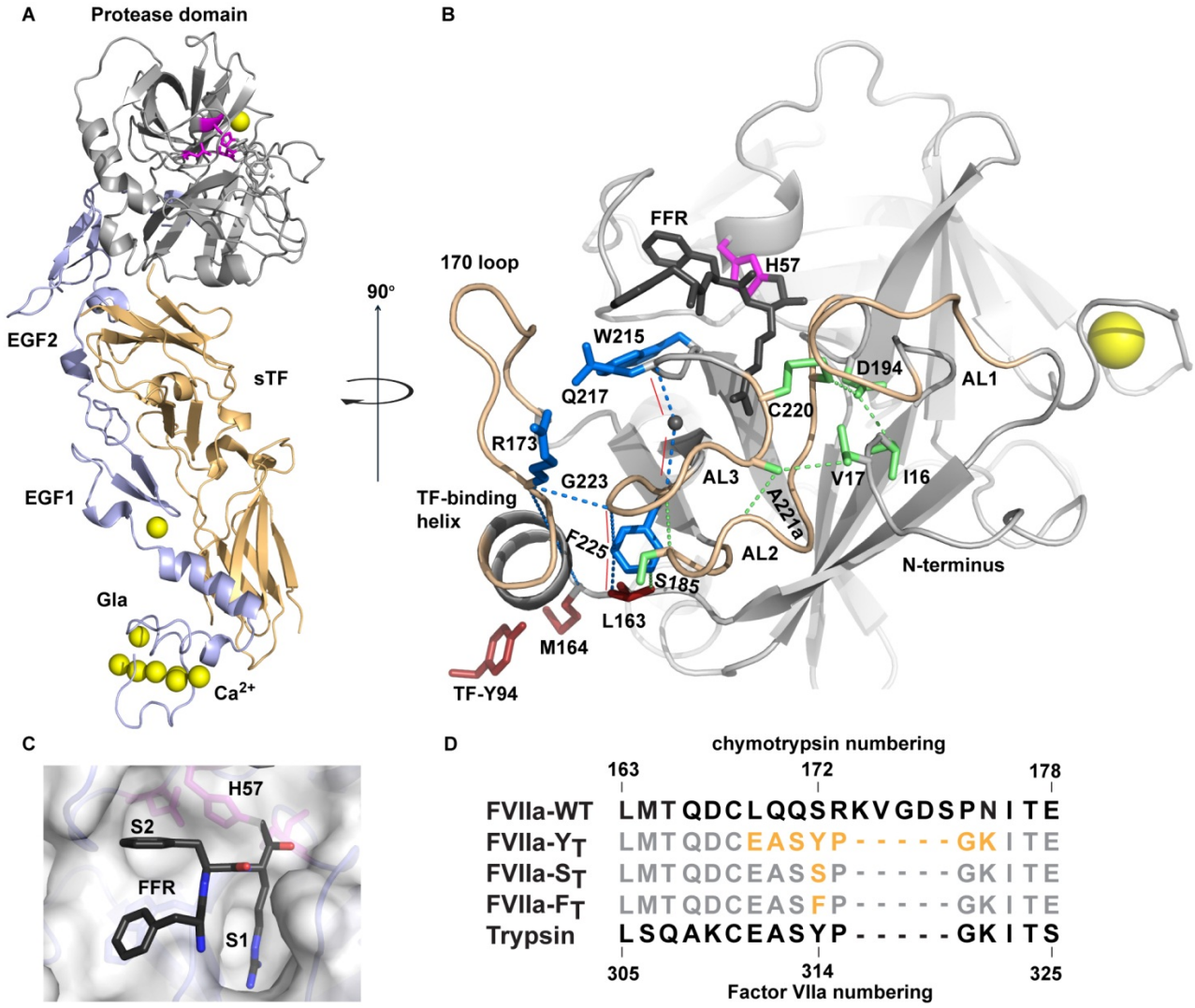

Figure 1

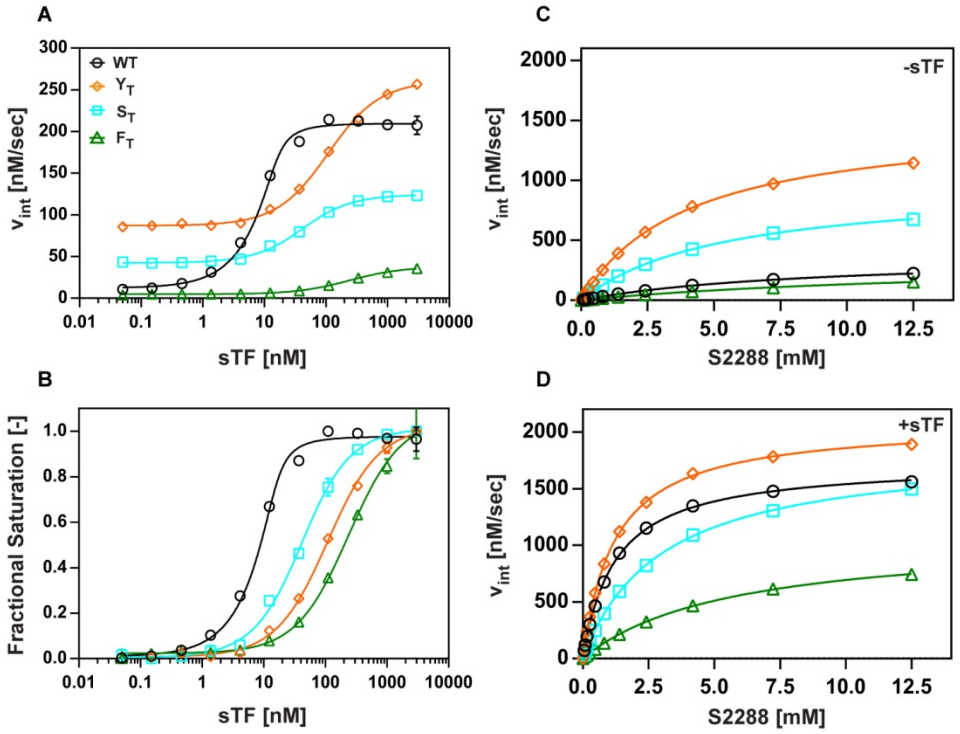

Figure 2

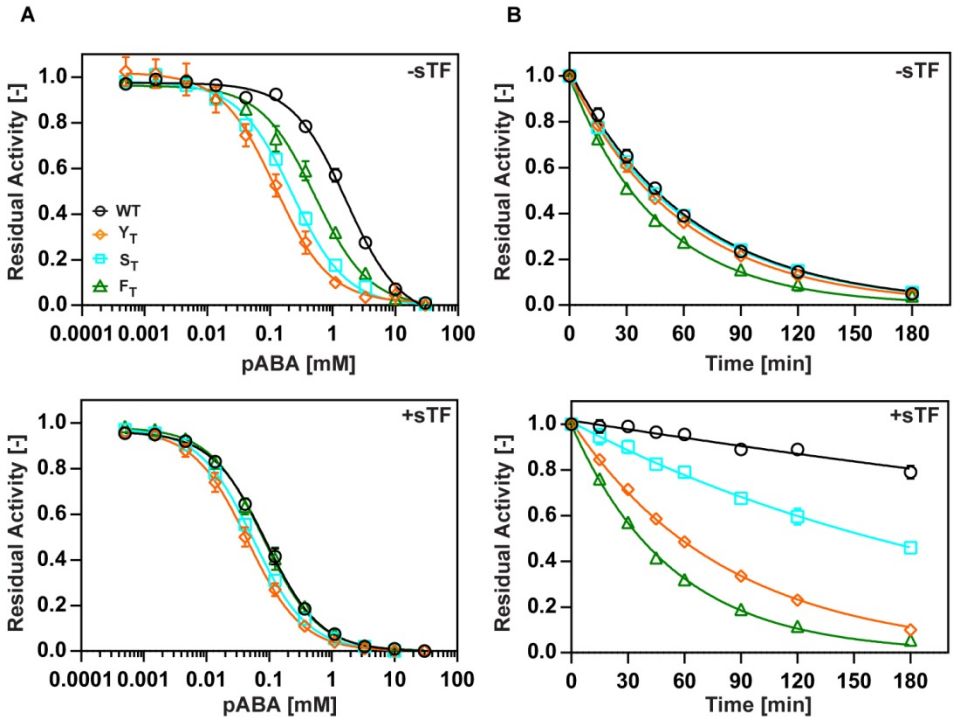

Figure 3

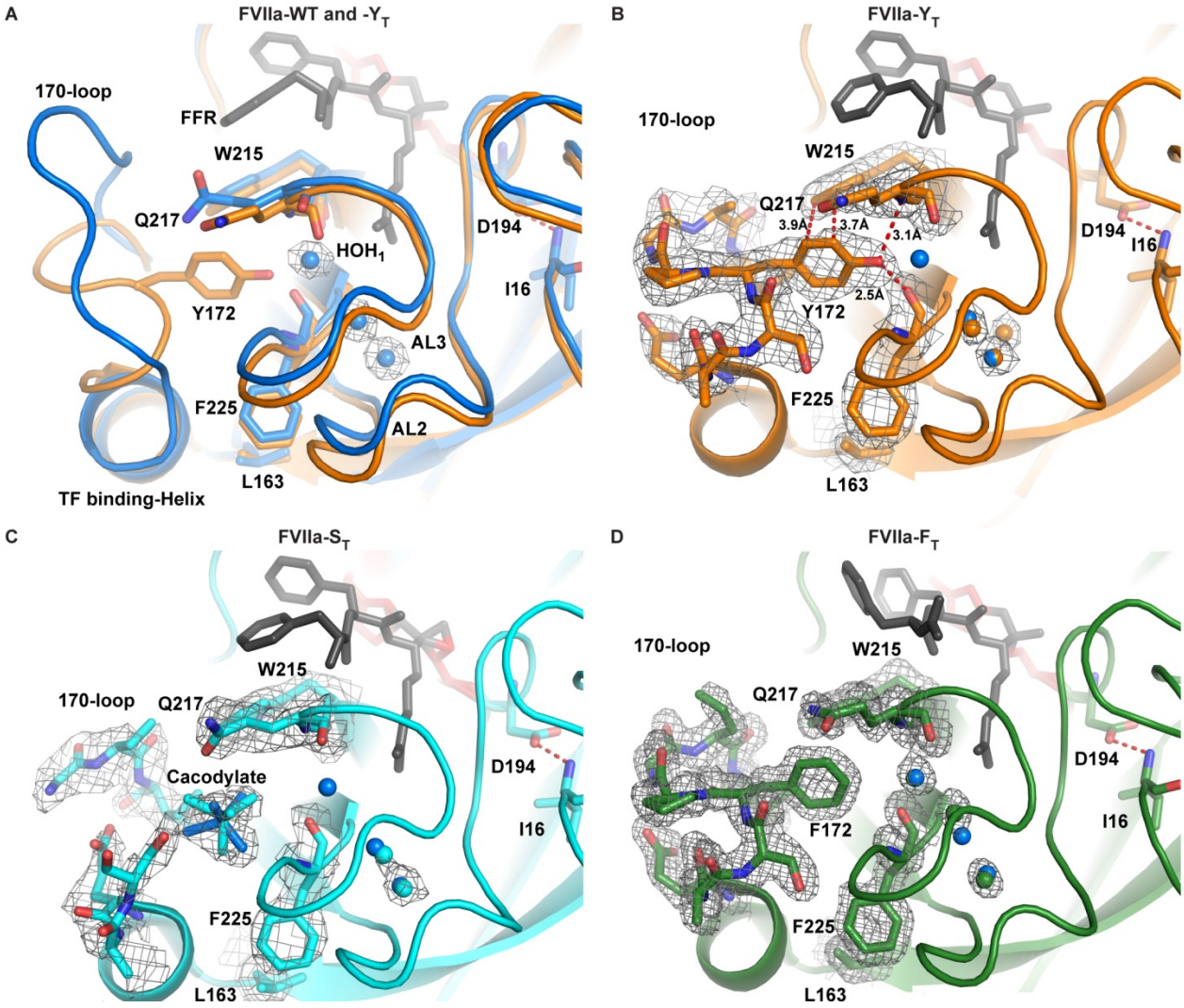

Figure 4

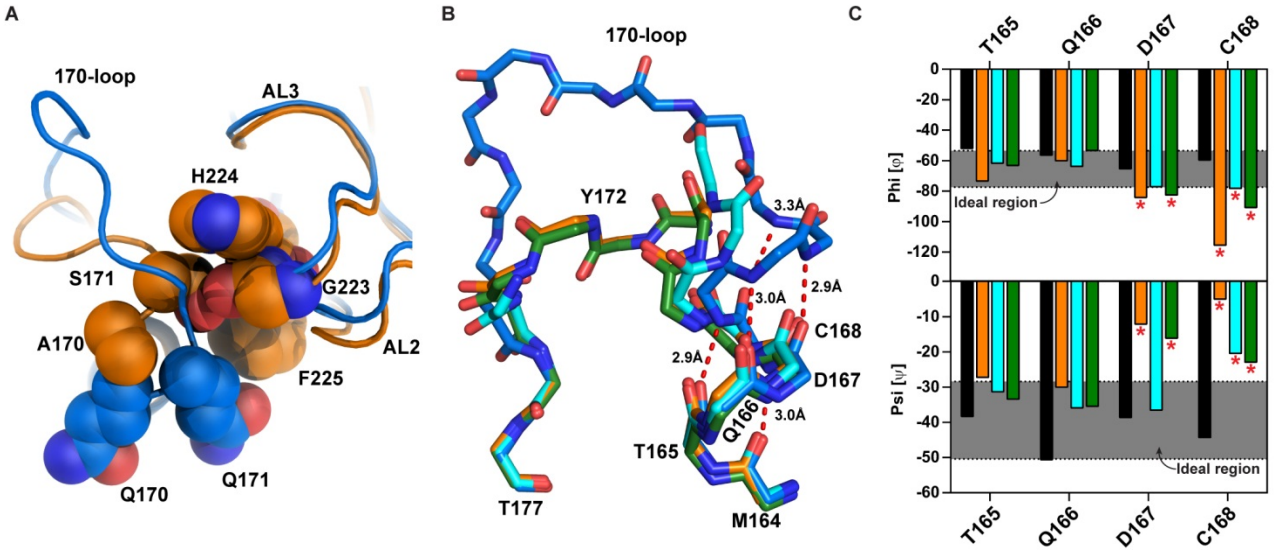

Figure 5

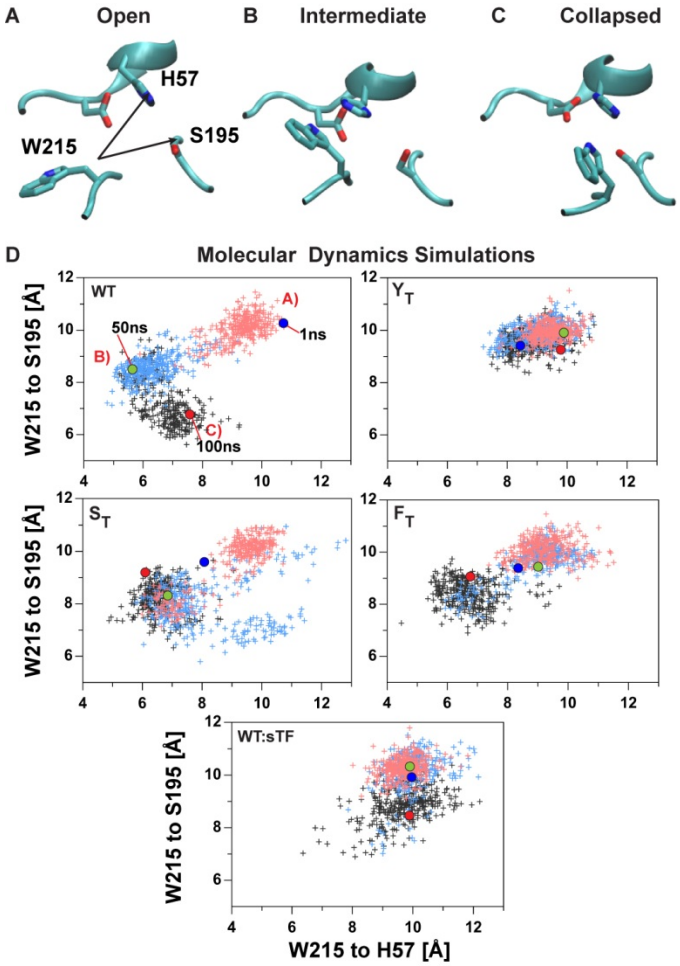

Figure 6

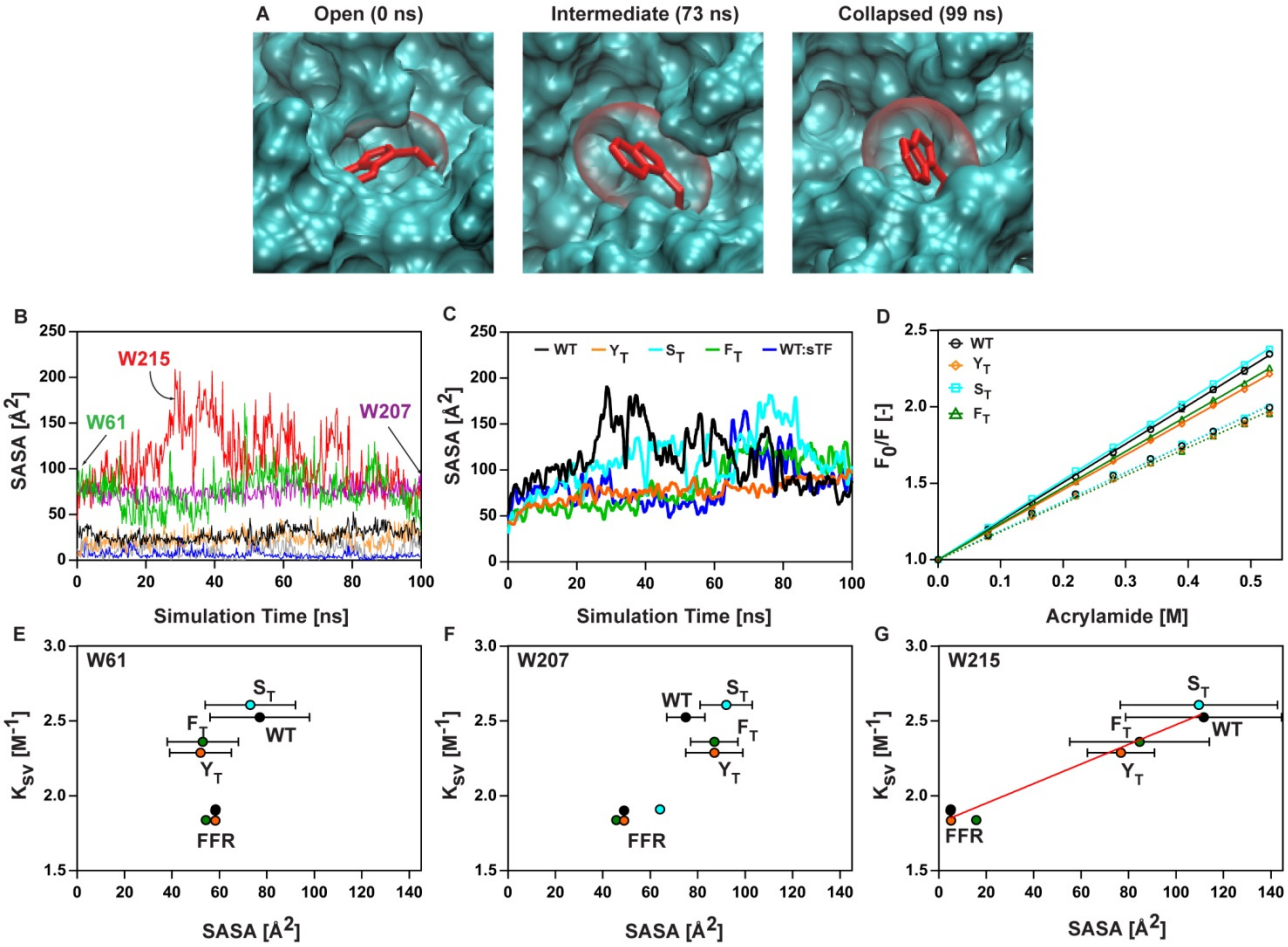

Figure 7

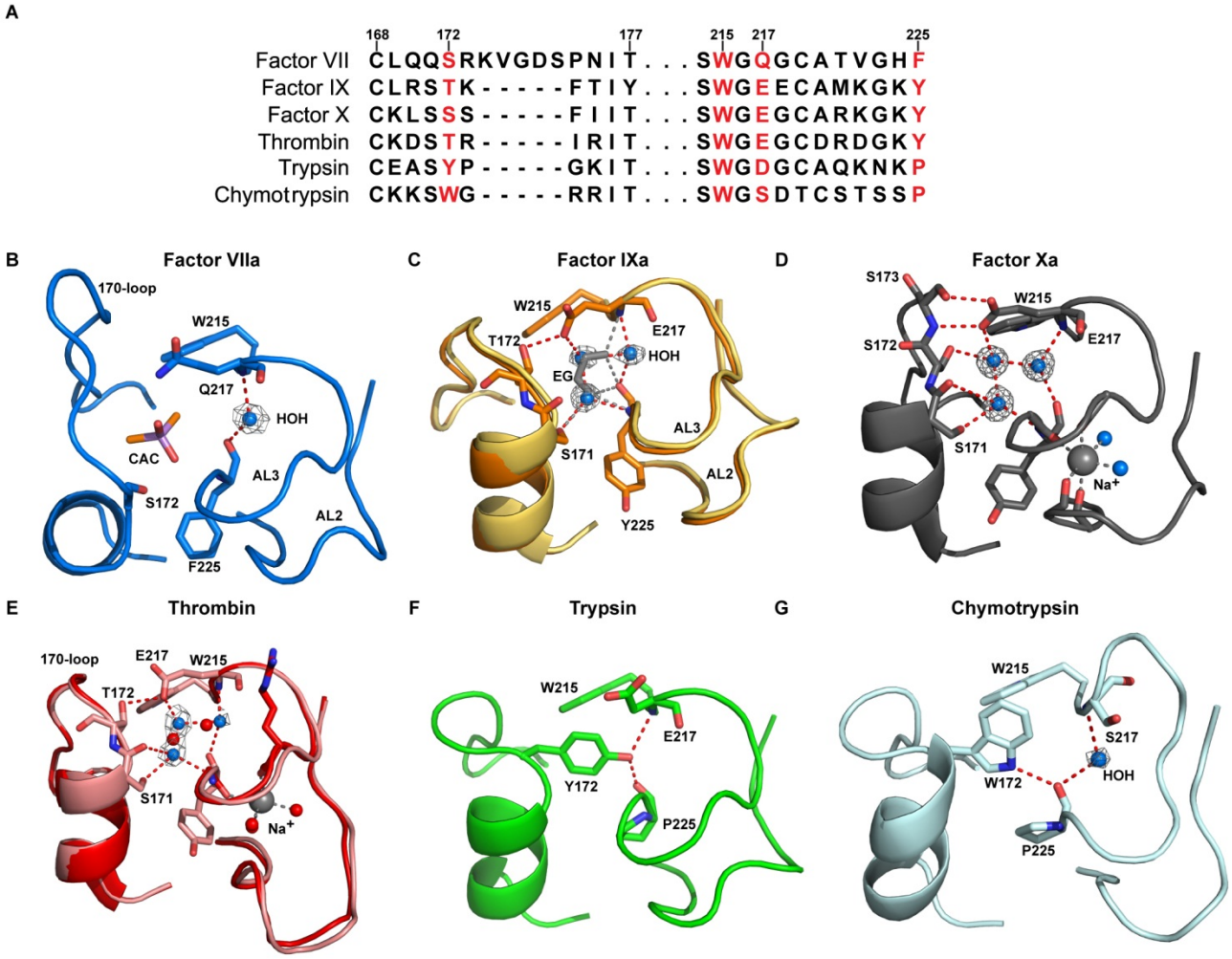

Figure 8

Molecular Basis of Enhanced Activity in Factor VIIa-Trypsin Variants Conveys Insights into Tissue Factor-Mediated Allosteric Regulation of Factor VIIa Activity

Anders B. Sorensen, Jesper J. Madsen, L. Anders Svensson, Anette A. Pedersen, Henrik Østergaard, Michael T. Overgaard, Ole H. Olsen and Prafull S. Gandhi

J. Biol. Chem. published online December 22, 2015
